Scientific Research Publishing

Journal of Electronics Cooling and Thermal Control, 2025, 14(1), 1-11
https://www.scirp.org/journal/jectc
ISSN Online: 2162-6170
ISSN Print: 2162-6162

Multifunctional Composite in the B_4C-SiC-TiC-TiB_2 System

Zviad Kovziridze, Natela Nijaradze, Maia Mshvildadze, Tamar Loladze, Nikoloz Loladze, Gulnazi Tabatadze, Teimuraz Cheishvili, Marina Kapanadze, Maia Balakhashvili, Veriko Qinqladze, Nino Darakhvelidze

Bionanoceramic and Nanocomposite Materials Science Center, Institute of Bionanoceramics and Nanocomposite Technology, Faculty of Chemical Technology and Metallurgy, Georgian Technical University, Tbilisi, Georgia
Email: kowsiri@gtu.ge

How to cite this paper: Kovziridze, Z., Nijaradze, N., Mshvildadze, M., Loladze, T., Loladze, N., Tabatadze, G., Cheishvili, T., Kapanadze, M., Balakhashvili, M., Qinqladze, V. and Darakhvelidze, N. (2025) Multifunctional Composite in the B_4C-SiC-TiC-TiB_2 System. *Journal of Electronics Cooling and Thermal Control*, **14**, 1-11.
https://doi.org/10.4236/jectc.2025.141001

Received: February 2, 2025
Accepted: March 28, 2025
Published: March 31, 2025

Abstract

Objective: To develop a composite material with enhanced technical and operational properties based on the B_4C-SiC-TiC-TiB_2 system. **Method:** The composite was fabricated via hot-pressing. Phase composition and microstructural characterization were performed using X-ray diffraction (DRON-3) and scanning electron microscopy (SEM). Mechanical properties were evaluated using a German R-100 tensile testing machine and a Rockwell hardness tester for hardness assessment. **Result:** The hot-pressing process induced a solid-state reaction between titanium carbide (TiC) and boron carbide (B_4C), leading to the *in-situ* formation of titanium diboride (TiB_2) grains, which contributed significantly to the composite's mechanical reinforcement. The addition of perlite facilitated the development of a glassy intergranular phase, forming continuous "bridges" between carbide grains, thereby enhancing grain boundary cohesion and mechanical stability. **Conclusion:** The synthesized composite demonstrates outstanding mechanical performance: **Flexural strength**: 389 MPa; **Compressive strength**: 1923 MPa; **Impact toughness**: 11.2 kJ/m^2. These properties make the material well-suited for wear-resistant applications operating under high-impact, thermomechanical loading and other conditions.

Keywords

Composite, Correlation, Porous Phase, Mechanical Strength, Structure

1. Introduction

The development and implementation of new technologies are currently considered

fundamental prerequisites for creating competitive, multifunctional materials, advancing integrated materials science, and promoting national economic development.

High-temperature, heteromodular, advanced ceramic composite materials are exemplary in this regard. These materials are characterized by superior physical and mechanical properties (such as hardness, strength limits, fracture toughness, and modulus of elasticity), excellent technological properties (such as good machinability with cutting tools), and outstanding operational performance (including wear resistance, resistance to static and dynamic loading, radiation resistance, and more).

The foundation for producing such materials lies in the use of refractory compounds, including: boron carbide, boron nitride, tantalum carbide, zirconium, aluminum, and yttrium oxides, silicon nitride, silicon carbide, titanium and zirconium borides, and carbides of titanium, tungsten, and tantalum. These compounds exhibit high thermodynamic stability, exceptional hardness, and wear resistance—properties they retain even under elevated temperature conditions. This thermal resilience is one of the key factors enabling their effective application in demanding technological environments.

2. Main Section

This study focuses on the synthesis and investigation of composite ceramic materials based on boron carbide (B_4C) and silicon carbide (SiC). For the fabrication of the composite, the following initial composition (in wt.%) was selected: B_4C—60%, SiC—20%, TiC—13%, Perlite—3% (appendage).

The selection of these compounds was driven by their unique combination of properties, including high hardness, high melting point, excellent corrosion resistance, wear resistance, and low density.

However, unlike other advanced ceramics, they exhibit low fracture toughness and impact resistance, which limits their broader application despite their advantageous properties. Numerous studies have been devoted to the development of composites based on these compounds for various purposes, particularly in armor applications, due to their low density [1]-[13].

In addition to boron carbide and silicon carbide, titanium carbide (TiC) was introduced into the composition. This inclusion was based on the known reaction that occurs between titanium carbide and boron carbide during high-temperature processing, resulting in the in-situ formation of titanium diboride (TiB_2), as confirmed by X-ray diffraction analysis (**Figure 1**). Titanium diboride is also known for its excellent mechanical properties.

The aim of this study was to achieve a highly dispersed and uniform distribution of the newly formed TiB_2 grains within the composite matrix. This uniform distribution is facilitated by an amorphous glassy phase formed by volcanic perlite, which acts as a bonding medium between the grains (**Figure 2**).

The chemical composition of perlite is as follows (wt.%):

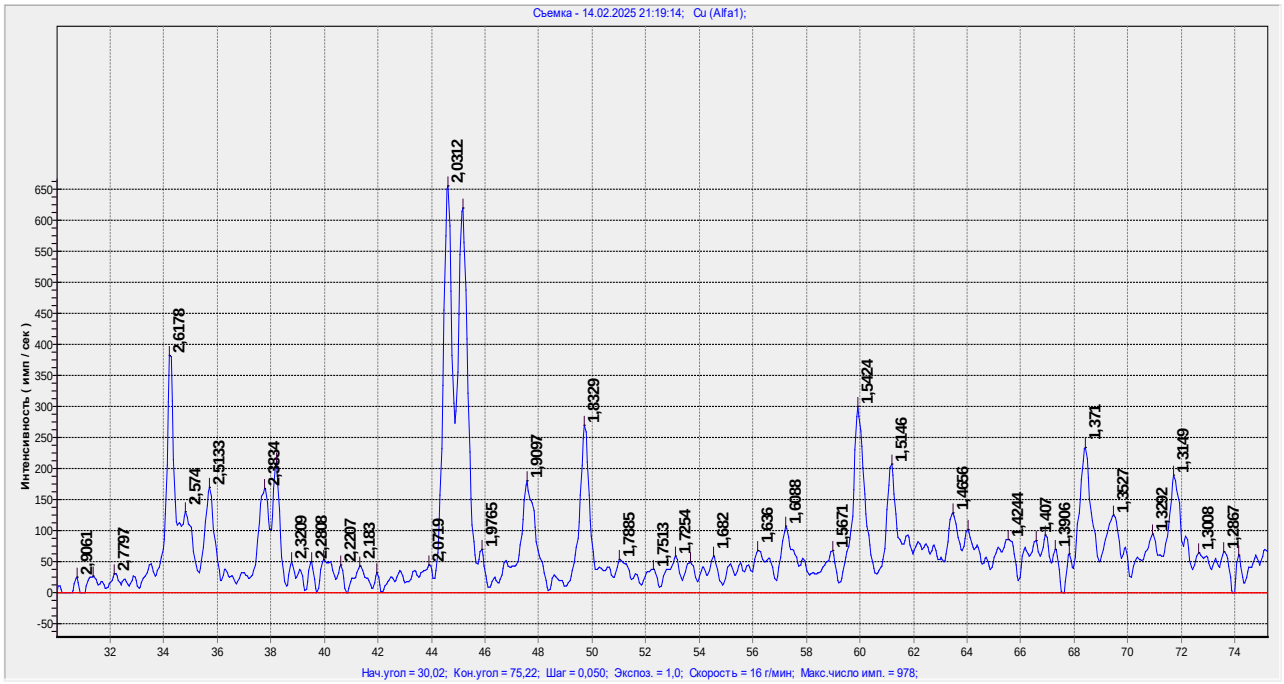

Figure 1. X-ray diffraction pattern of the obtained composite. TiB_2—dhkl—1.3149; 1.371; 1.5146; 1.6088; 2.0312; 2.6178 Å. SiC—dhkl—1.5424; 1.9097; 2.3834; 2.5133; 2.574 Å. B_4C—dhkl—238 Å.

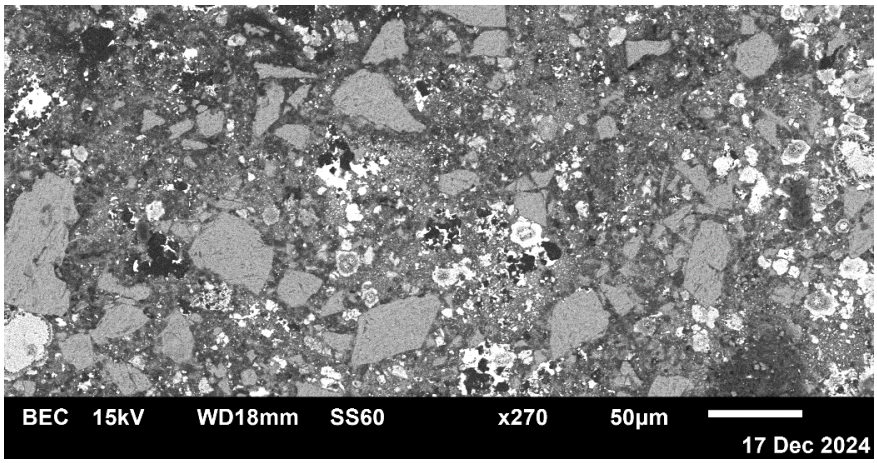

Figure 2. Microstructure of the composite.

- SiO_2—72.11
- Al_2O_3—15.56
- Fe_2O_3—0.53
- CaO—0.71
- MgO—0.35
- K_2O—4.87
- Na_2O—3.27
- Loss on ignition—3.03

The melting point of perlite is approximately 1240˚C. It contains 76 wt.% glassy phase, with the remainder consisting of crystalline phases and gases trapped

during the rapid cooling of erupted lava. Its density ranges from 2.3 to 2.4 g/cm^3.

3. Method

Structural-morphological and elemental composition of the samples was examined using a JEOL JSM-6510LV scanning electron microscope, manufactured in Japan, equipped with an Oxford Instruments X-MaxN energy-dispersive X-ray spectroscopy (EDS) system. Surface imaging was performed using both secondary electrons (SEI) and backscattered electrons (BES) under an accelerating voltage of 20 kV. In certain cases, to reduce surface charging, samples were coated with a ~10 nm Pt layer using a JEOL JEC-3000FC vacuum sputter coater.

4. Results

The results of the morphological analysis of the polished sample surface are presented in Figure 2. Gray silicon carbide and white boron carbide grains are clearly distinguishable. Newly formed titanium diboride is also observed between them, the presence of which is confirmed by microspectral and electron imaging data (Figure 3, Figure 4).

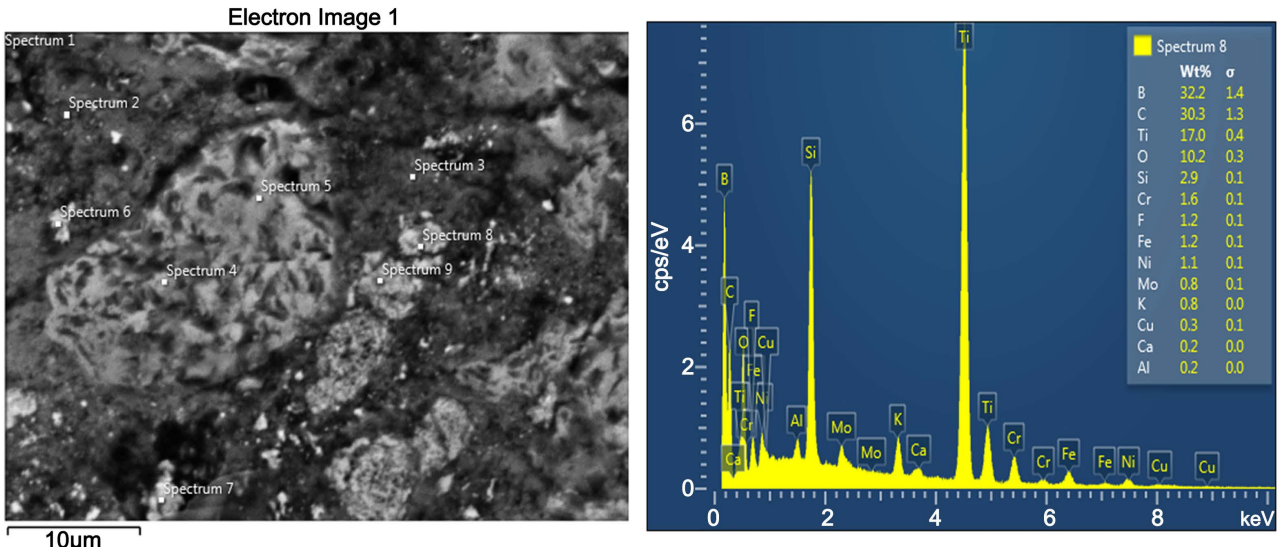

Figure 3. Micro X-ray spectral images of the investigated composite.

To examine the fracture mechanism of the composite at the microscopic level, a freshly fractured sample was prepared, and its fracture surface was analyzed using a scanning electron microscope (SEM). SEM image of the fracture surface is presented in Figure 5.

Figure 5 illustrates that the morphological features are consistent and uniform throughout both the surface and the volume of the sample. The fracture mechanism is characterized by a combination of transcrystalline and ductile modes. Furthermore, the crystals exhibit stepwise fracture, which effectively impedes crack

propagation. This behavior is corroborated by the mechanical strength data presented in Table 1.

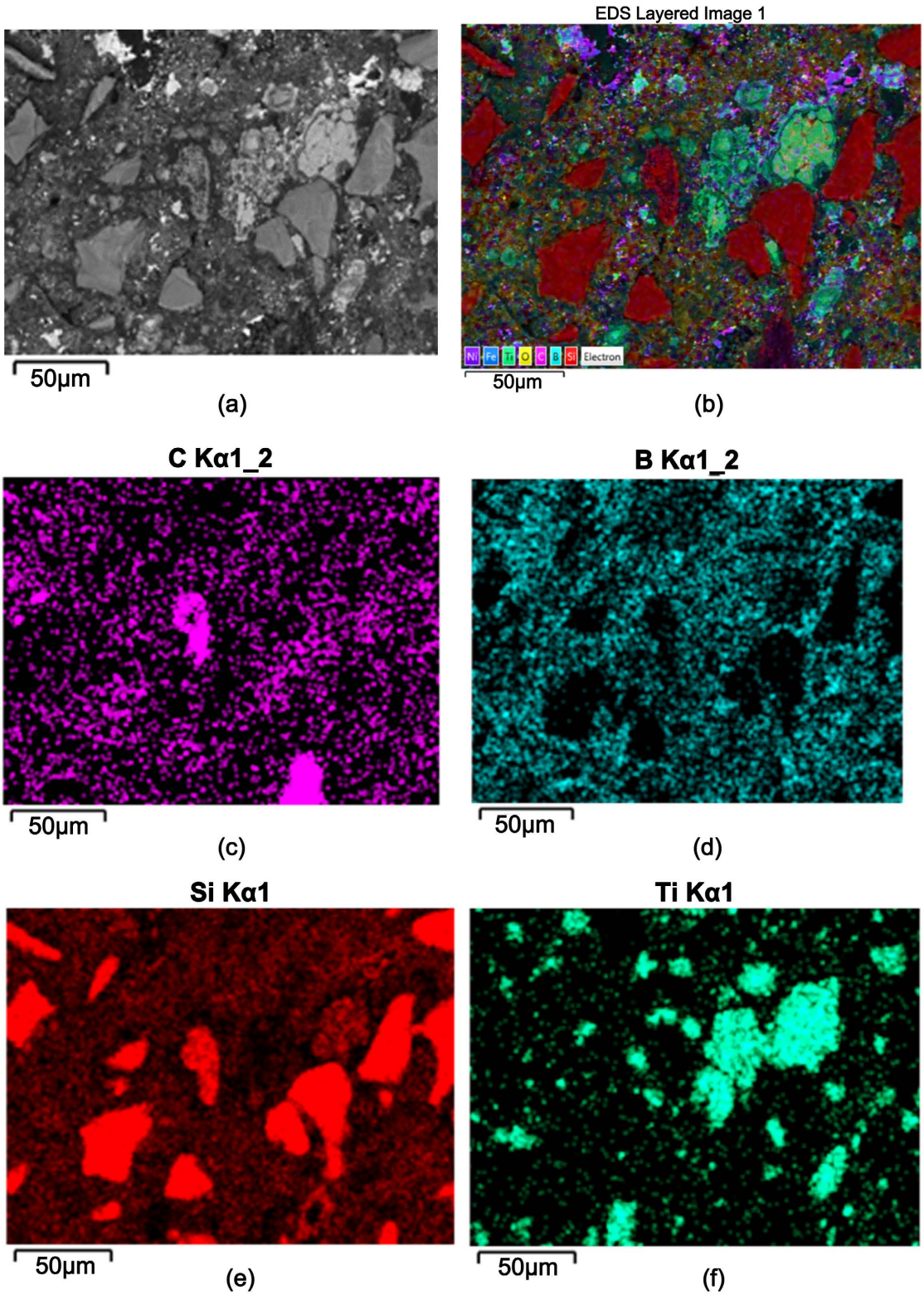

Figure 4. SEM images illustrating the spatial phase distribution within the composite.

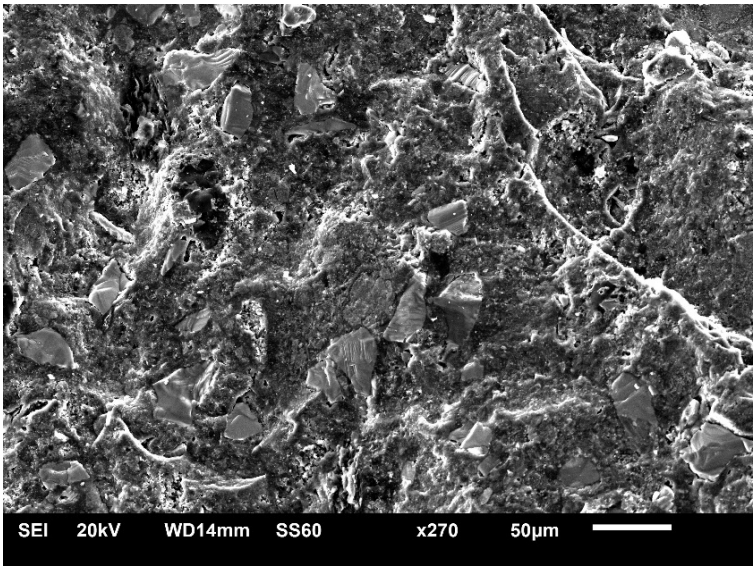

Figure 5. Fracture surface SEM micrograph of the studied composite.

5. Discussion

As observed in **Figure 4**, titanium diboride forms a shell around the silicon carbide grains. In the event of crack initiation within a carbide grain, it localises the crack and reduces its propagation rate [1]. Additionally, unreacted boron carbide and titanium diboride grains are interconnected by thin amorphous glassy bridges [2]. The composite was fabricated using the hot-pressing method at 1620˚C. The physical and technical properties of the composite are presented in **Table 1**.

Table 1. Physical and technical characteristics of the composite.

Composite B_4C-SiC-TiB_2-Perlite	Theoretical density, Υ_{th}, g/cm^3	Relative density, Υ_r	Open porosity п, %	Hardness, HRA	Compressive strength, σ_c. MPa	Flexural strength, σ_B. MPa	Impact toughness, A kJ/m^2
	3.1	0.96	<1.0	91	1923	389	11.2

As shown in **Table 1**, the obtained composite is characterized by high physical and mechanical properties and low volume porosity, which enhances its application potential. To further characterize the composite, Z. Kovziridze's formulas describing the dependence of mechanical properties on the porous phase and the correlation between the morphology of the crystalline phase and macromechanical characteristics were applied [14]. For this purpose, the morphology of pores and crystals was examined using microstructural images. The data presented in **Table 2** and **Table 3** were utilized as input for the corresponding formulas.

Table 2. Porous phase morphology.

Visual field area, S, mkm^2	Total pore area, S, μM^2	Maximum pore size, D_{max}, μM	Minimum pore size, D_{min}, μM	Pore shape factor, $F_p = D_{max}/D_{min}$	Pore distribution factor in the matrix, P_d	Volume fraction of the porous phase, P_{vol}, %	Average pore size, P_m, μM	Load under bending, P, MPA
36,500	303	10	5	2	0.9	0.83	7	389

Table 3. Crystalline phase morphology.

Visual field area, S, μM^2	Total crystal area, S_{cryst}, μM^2	Maximum crystal size, D_{max}, μM	Minimum crystal size, D_{min}, μM	Crystal shape factor, $F_{kf} = D_{max}/D_{min}$	Crystal distribution factor in the matrix, F_{kd}	Volume fraction of the crystalline phase, K_v, %	Average crystal size, K_m, μM	Load under bending, P_{MPa}
36,500	36,197	18	4	4.5	0.9	89.17	6	389

$$\sigma_{m/p} = P/F_p \cdot P_d \cdot P_{vol} \cdot P_m$$

where:

P—applied load in bending mechanics (MPa);

F_p—pore shape factor;

P_d—pore distribution factor in the matrix;

P_{vol}—volume fraction of the porous phase in the matrix;

P_m—average pore size.

$$\sigma_{m/p} = P/F_p \cdot P_d \cdot P_{vol} \cdot P_m = 389/2 \times 0.9 \times 0.83 \times 7 = 389/10.46 = 37.2 \text{ MPa}.$$

$$\sigma_d = PF_{kd}/K_m K_v F_{kf}$$

where:

P—applied load in bending or compression mechanics (MPa);

F_{kd}—crystal distribution factor in the matrix;

K_m—average crystal size (μm);

K_v—volume fraction of crystals in the matrix (wt.%);

F_{kf}—crystal shape factor.

$$\sigma_d = P \times F_{kd}/K_m K_v F_{kf} = 389 \times 0.9/6 \times 89.17 \times 4.5 = 389 \times 0.9/2407.6 = 0.17$$

$$\sigma_d = P \times F_{kd}/K_m K_v F_{kf} = 1923 \times 0.9/6 \times 89.17 \times 4.5 = 1730.7/2407.6 = 0.72$$

The formula accounts for both volumetric and surface defects of crystals, as well as the micro- and macrostructural volumetric and surface morphology of the crystalline phase, its distribution within the matrix, and the transformations occurring due to chemical and physicochemical processes during material consolidation. These properties are determined experimentally.

Notably, the proposed formula is applicable to a wide range of ceramic materials and ceramic composites, including metal-ceramics, bio ceramics, glass-ceramics, and glass-metal-ceramics. It captures the relationship between the macro mechanical properties of these materials, specifically, their ultimate failure characteristics, and key morphological parameters of the crystalline phase, such as crystal size, shape, distribution, and volume fraction within the matrix, as well as the crystal shape factor. In addition, the formula accounts for the contribution of the most mechanically robust phase in the consolidated material, reflecting its critical role in determining the overall performance characteristics essential for industrial application and long-term service reliability.

During thermal treatment, key factors influencing the final properties of ceramic materials include the dynamics of crystal formation, their spatial distribution within the matrix, and the evolution of crystal morphology. These aspects,

thoroughly examined in this study, are closely linked to the physicochemical processes that occur under thermal stress. The proposed formula offers a comprehensive framework for modeling the correlation between the morphology of the crystalline phase and the macro mechanical properties of ceramic components. Its applicability extends to all types of ceramics and ceramic composites employed in advanced technologies, diverse engineering sectors, and everyday applications.

The B_4C-TiC-SiC-TiB_2-perlite composite, which demonstrates high mechanical and operational properties, was fabricated via hot pressing at a temperature of 1620˚C. However, as the results indicate, the correlation is not strong. This may be attributed to the high crystal shape factor. Notably, attrition milling and planetary ball milling of the mixture were deliberately avoided, maintaining the materials' original dispersion. The disparity between the smallest and largest particles was substantial, which significantly contributed to the reduction in correlation. Consequently, the correlation coefficient was found to be 0.17 for bending and 0.72 for compression.

Ideally, the crystal shape factor should not exceed 3, and the crystal size should preferably remain within the range of 7 - 8 microns, while also being uniformly distributed throughout the matrix. Experimental evidence shows that fine-grained samples exhibit higher strength compared to coarse-grained ones [15]-[19], since the length of Griffith microcracks is determined by grain size. This phenomenon is presumably related to stress accumulation at grain boundaries caused by anisotropic thermal expansion [20]-[28].

6. Electrical Properties

The volume and surface electrical resistivity (ρ_v and ρ_s) of the obtained material was experimentally determined as a function of temperature in the range of 25˚C - 300˚C. Measurements were conducted using a specially designed thermally controlled cell, simultaneously on two samples, with an electronic ohmmeter employed for resistance measurements. The test samples were disk-shaped, with a diameter-to-height ratio of approximately D/H ≈ 5. Air-dried samples (25˚C, relative humidity 47.5%) were placed in the measurement cell, and their volume (R_v) and surface (R_s) resistance values (Ω) were recorded. Subsequent measurements in the temperature range of 100˚C - 300˚C were performed at 50˚C intervals. Using the corresponding calculations, specific resistivity values ρ_v (Ω·m) and ρ_s (Ω) were obtained. The resulting "$\rho_{v,s} - t$" relationships are presented in **Figure 6**.

It was established that the variation of volume resistivity (ρ_v) with temperature is linear, and within the 25˚C - 300˚C interval, a nearly twofold decrease in specific resistivity is observed. A noteworthy behavior is exhibited by the surface resistivity (ρ_s), whose values were determined under conditions of reversible temperature cycling in the range of 25˚C - 300˚C. For the initial sample (Curve 2), the ρ_s values were relatively high at room temperature, showed a sharp decline in the range of 25˚C - 150˚C, and subsequently aligned with the ρ_v values. During the cooling phase (Curve 2'), ρ_s values closely matched those of ρ_v, with only a minor deviation (≈1 Ω).

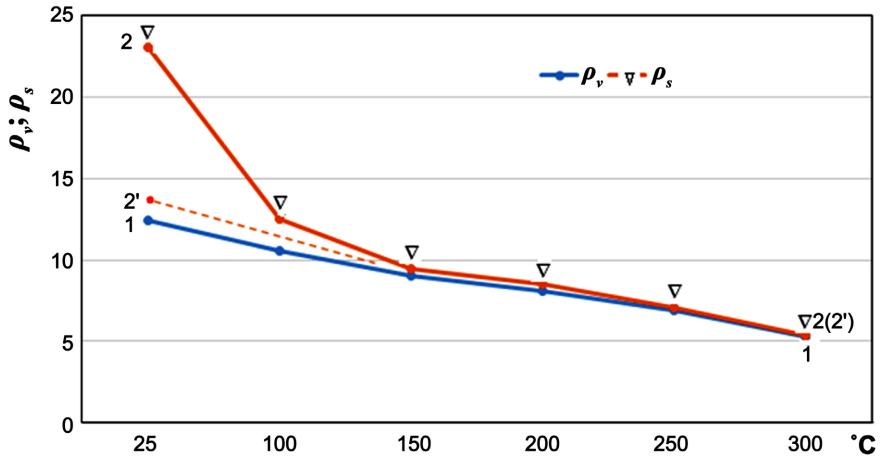

Figure 6. Temporal dependencies of the material's volumetric density (ρ_v) (curve 1) and surface density (ρ_s) (curves 2 and 2').

The distinct behavior of the "$\rho_s - t$" curve under temperature reversal is likely attributable to condensed moisture on the surface of the initial sample, which evaporated during heating, leading to the convergence of ρ_s and ρ_v values at higher temperatures.

The key electrical properties of the investigated material, calculated across the temperature range of 25˚C - 300˚C, are presented in Table 4.

Table 4. Principal electrical characteristics of the studied material.

N	Electrical Properties			
	Title	Conventional Symbol	Unit of Measurement	Values
1	Temperature Coefficient of Electrosensitivity	B	Ω·m·K	529.1
2	Temperature Coefficient of Electrical Resistivity	$\Delta\alpha_T$	$\Omega\cdot m\cdot K^{-1}$	-2.7×10^{-3}
3	Activation Energy of Electrical Conductivity	ΔE	eV	0.334

The resulting material, primarily composed of titanium, silicon, and boron carbides, well-known for their electrical properties, exhibits electrical behavior characteristic of semiconductor materials.

7. Conclusions

During the hot pressing at 1620˚C, a reaction occurred between titanium carbide and boron carbide, resulting in the formation of titanium diboride. This reaction contributed to a significant enhancement of the composite's mechanical properties. Additionally, the presence of perlite in the composite led to the formation of a glassy phase that creates so-called "bridges" with the carbide grains, further improving the mechanical performance of the material. A clear correlation was

established between the matrix composition and the mechanical properties of the material, specifically showing the dependence of mechanical characteristics on the content of the porous phase.

The resulting composite in the B_4C-SiC-TiC-TiB_2 system, doped with 3 wt.% glassy perlite, primarily composed of titanium, silicon, and boron carbides known for their electrical properties, exhibits electrical behavior characteristic of semiconductor materials.

Conflicts of Interest

The authors declare no conflicts of interest regarding the publication of this paper.

References

[1] Lensky, V.V., Chikina, A.A., *et al.* (2008) Development of Armor Shells for Personal Protective Equipment from Reaction-Bonded Silicon Carbide. *Scientific and Technical Collection, Issues of Defense Technology*, **15**, 148-149.

[2] Google Patents (1974) Method for Producing a Ceramic Armor Material Based on Silicon Carbide and Boron Carbide, US Patent 3,796,564, Class C22C 1/04.

[3] Google Patents (2004) Composite Ceramic Material, US Patent 6,805,034, Class F41H 5/00.

[4] Wang, B., Cai, D., Wang, H., Zou, W., Yang, Z., Duan, X., *et al.* (2023) Microstructures and Mechanical Properties of B_4C-SiC and B_4C-SiC-TiB_2 Ceramic Composites Fabricated by Hot Pressing. *Journal of the American Ceramic Society*, **106**, 5046-5066. https://doi.org/10.1111/jace.19136

[5] Kovziridze, Z., Mestvirishvili, Z. and Tabatadze, G. (2012) Influence of TiB_2 and ZrB_2 Additives on the Properties of Boron Carbide. *Ceramics*, **27**, 33-39.

[6] Srivatsan, T.S., Guruprasad, G., Black, D., Radhakrishnan, R. and Sudarshan, T.S. (2005) Influence of TiB_2 Content on Microstructure and Hardness of TiB_2-B4C Composite. *Powder Technology*, **159**, 161-167. https://doi.org/10.1016/j.powtec.2005.08.003

[7] Huang, S.G., Vanmeensel, K., Malek, O.J.A., Van der Biest, O. and Vleugels, J. (2011) Microstructure and Mechanical Properties of Pulsed Electric Current Sintered B_4C-TiB_2 Composites. *Materials Science and Engineering*: *A*, **528**, 1302-1309. https://doi.org/10.1016/j.msea.2010.10.022

[8] Kriener, M., Muranaka, T., Kato, J., Ren, Z., Akimitsu, J. and Maeno, Y. (2008) Superconductivity in Heavily Boron-Doped Silicon Carbide. *Science and Technology of Advanced Materials*, **9**, Article 044205. https://doi.org/10.1088/1468-6996/9/4/044205

[9] Kovziridze, Z., Nizharadze, N., Tabatadze, G., Nikoleishvili, E., Mestvirishvili, Z. and Kinkladze, V. (2011) Multifunctional Hetero-Modulus Composites in the B_4C-BN-TiC-SiC-C System. *Journal of the European Ceramic Society*, **31**, 1921-1926. https://doi.org/10.1016/j.jeurceramsoc.2011.01.017

[10] Kovziridze, Z., Nijaradze, N., Tabatadze, G., Mshvildadze, M., Nikoleishvili, E. and Mestvirishvili, Z. (2013) Improvement of Boron Carbide Mechanical Properties in B_4C-TiB_2 and B_4C-ZrB_2 Systems. *Journal of Electronics Cooling and Thermal Control*, **3**, 43-48.

[11] Kovziridze, Z., Nijharadze, N., Tabatadze, G. and Mestvirishvili, Z. (2013) Ceramic Composite in the Al_2O_3-B_4C-TiC System. *Journal of the Georgian Ceramicists*

Association "*Ceramics*", **13**, 19-22.

[12] Kovziridze, Z., Nijaradze, N., Tabatadze, G., Cheishvili, T., Mshvildadze, M., Kapanadze, M., Balakhashvili, M. and Daraxvelidze, N. (2024) Smart Nanocomposite in the SiC-Si-Al-Al_2O_3-Geopolymer System. *International Journal of Innovative Research in Multidisciplinary Education*, **3**, 1121-1136. https://doi.org/10.58806/ijirme.2024.v3i6n28

[13] Kovziridze, Z., Nijharadze, N., Tabatadze, G., *et al.* (2018) Synthesis of Self-Healing Composites by Reactive Sintering in the SiC-B_4C-Si-Al-Al_2O_3 System via Metallothermal and Nitriding Processes. *Ceramics and Advanced Technologies*, **20**, 13-17.

[14] Kovziridze, Z., Nijharadze, N., Tabatadze, G., Mestvirishvili, Z. and Darakhvelidze, N. (2019) Investigation of the Phase Composition of Composites in the SiC-B_4C-Si-Al-Al_2O_3 System. *Ceramics and Advanced Technologies*, **21**, 44-51.

[15] Kovziridze, Z. (2022) Sintering Physics and Kinetics. Technical University.

[16] Griffith, A.A. (1924) The Theory of Rupture. In: Waltman, J., Ed., *Proceedings of the First International Congress for Applied Mechanics Delft*, Delft, 55-63.

[17] Griffith, A.A. (1920) Studying the Strength of Glass Fibers. *Philosophical Transactions of the Royal Society*, **A221**, 163.

[18] Inglis, C.E. (1913) Calculation of Stress Concentrations at the Crack Edge. *Transactions of the Institution of Naval Architects*, **55**, Article 219.

[19] Orowan, E. (1934) Die mechanischen Festigkeitseigenschaften und die Realstruktur der Kristalle. *Zeitschrift für Kristallographie—Crystalline Materials*, **89**, 327-343. https://doi.org/10.1524/zkri.1934.89.1.327

[20] Charles, R.J. (1958) Static Fatigue of Glass. *Journal of Applied Physics*, **29**, 1549-1553. https://doi.org/10.1063/1.1722991

[21] Baker, T.C. and Preston, F.W. (1946) Fatigue of Glass under Static Loads. *Journal of Applied Physics*, **17**, 170-178. https://doi.org/10.1063/1.1707702

[22] Kovziridze, Z. (2018) Formula for the Dependence of Macromechanical Properties on the Porous Phase. Sakpatent (Georgian Patent), Certificate No. 7276.

[23] Kovziridze, Z., Aneli, J., Nijaradze, N. and Tabatadze, G. (2017) Ceramic and Polymer Composites. Lambert Academic Publishing.

[24] Kovziridze, Z., Nijharadze, N., Tabatadze, G. and Aneli, J. (2016) Ceramic and Polymer Composites. Lambert Academic Publishing, 419-421.

[25] Kovziridze, Z., Nijharadze, N., Tabatadze, G. and Darakhvelidze, N. (2017) Self-Healing and Low-Tungsten Composite Materials. Georgian Technical University, 153-171.

[26] Kovziridze, Z., Nijharadze, N. and Tabatadze, G. (2014) High-Strength Heteromodular Composites. Georgian Technical University, 41-50.

[27] Kollenberg, W. (2004) Technische Keramik. Vulkan-Verlag ESSEN, 230-290.

[28] Kovziridze, Z., Nijaradze, N., Tabatadze, G., Cheishvili, T., Mshvildadze, M., Mestvirishvili, Z., *et al.* (2017) Obtaining of Sialon Composite via Metal-Thermal and Nitrogen Processes in the Sic-Si-Al-Geopolymer System. *Journal of Electronics Cooling and Thermal Control*, **7**, 103-122. https://doi.org/10.4236/jectc.2017.74009